

## How the Shape of Pre- and Postsynaptic Signals Can Influence STDP: A Biophysical Model

**Ausra Saudargiene**

*ausra@cn.stir.ac.uk*

*Department of Psychology, University of Stirling, Stirling FK9 4LA, Scotland, and  
Department of Informatics, Vytautas Magnus University, Kaunas, Lithuania*

**Bernd Porr**

*Bernd.Porr@cn.stir.ac.uk*

**Florentin Wörgötter**

*worgott@cn.stir.ac.uk*

*Department of Psychology, University of Stirling, Stirling FK9 4LA, Scotland*

Spike-timing-dependent plasticity (STDP) is described by long-term potentiation (LTP), when a presynaptic event precedes a postsynaptic event, and by long-term depression (LTD), when the temporal order is reversed. In this article, we present a biophysical model of STDP based on a differential Hebbian learning rule (ISO learning). This rule correlates presynaptically the NMDA channel conductance with the derivative of the membrane potential at the synapse as the postsynaptic signal. The model is able to reproduce the generic STDP weight change characteristic. We find that (1) The actual shape of the weight change curve strongly depends on the NMDA channel characteristics and on the shape of the membrane potential at the synapse. (2) The typical antisymmetrical STDP curve (LTD and LTP) can become similar to a standard Hebbian characteristic (LTP only) without having to change the learning rule. This occurs if the membrane depolarization has a shallow onset and is long lasting. (3) It is known that the membrane potential varies along the dendrite as a result of the active or passive backpropagation of somatic spikes or because of local dendritic processes. As a consequence, our model predicts that learning properties will be different at different locations on the dendritic tree. In conclusion, such site-specific synaptic plasticity would provide a neuron with powerful learning capabilities.

### 1 Introduction ---

Hebbian (correlation-based) learning requires that pre- and postsynaptic spikes arrive within a certain small time window, which leads to an increase of the synaptic weight (Hebb, 1949). Originally it had been supposed that the temporal order of both signals is irrelevant (Bliss & Lomo, 1970, 1973;

Bliss & Gardner-Edwin, 1973). However, rather early first indications arose that temporal order is indeed important (Levy & Steward, 1983; Gustafsson, Wigstrom, Abraham, & Huang, 1987; Debanne, Gahwiler, & Thompson, 1994). Later, this was termed spike-timing-dependent plasticity (STDP), which refers to the observation that many synapses will decrease in strength when the postsynaptic signal precedes the presynaptic signal (defined here as  $T < 0$ ), while they will grow if the temporal order is reversed (thus,  $T > 0$ ) (Markram, Lübke, Frotscher, & Sakmann, 1997; Magee & Johnston, 1997; Bi & Poo, 2001).  $T$  denotes the temporal interval between post- and presynaptic signals ( $T := t_{post} - t_{pre}$ ). This leads to the characteristic antisymmetrical weight change curve measured by several groups.

Antisymmetrical learning curves were first observed in the entirely different context of classical conditioning models requiring much slower time-scales. In their seminal study, Sutton and Barto (1981) introduced a learning rule based on the temporal difference between subsequent output signals, and they observed that this rule leads to inhibitory conditioning when the temporal order of conditioned and unconditioned stimulus is reversed. In their hands, this was an unwanted effect, because inhibitory conditioning is only very rarely observed in experiments (Prokasy, Hall, & Fawcett, 1962; Mackintosh, 1974, 1983; Gormezano, Kehoe, & Marshall, 1983). It gave, however, a hint that this class of "differential" algorithms would in general produce antisymmetrical learning curves. The TD learning rule (Sutton, 1988) also belongs to this class of algorithms. Accordingly, Rao and Sejnowski (2001) successfully used the TD algorithm to implement STDP. In the original TD learning rule, one specific signal is used as a dedicated reward, which is treated differently from the other inputs. Thus, Rao and Sejnowski (2001) had to change the TD rule to some degree in order to better adapt it to STDP (see also section 4). The differential Hebbian ISO learning rule, recently introduced by us (Porr & Wörgötter, 2003a) in the context of machine control (Porr & Wörgötter, 2003b), on the other hand, treats all input lines equivalently. This prompted us to query if the ISO rule could also be applied to spiking neurons in a biophysically more realistic model of STDP.

The mechanisms that underlie STDP are associated with the biophysics of long-term potentiation (LTP) and long-term depression (LTD; Martinez & Derrick, 1996; Malenka & Nicoll, 1999; Bennett, 2000). This involves complex calcium dynamics and the concerted action of several enzymes such as  $\alpha$ -calcium-calmodulin-dependent protein kinase II (CaMKII; e.g., see Teyler & DiScenna, 1987). Several kinetic models have been made (Senn, Markram, & Tsodyks, 2000; Castellani, Quinlan, Cooper, & Shouval, 2001; Shouval, Bear, & Cooper, 2002) in order to arrive at a better understanding of some of these aspects, and some models reach a relatively high level of biophysical and biochemical complexity. As a consequence, however, they contain many degrees of freedom.

The question of STDP will be addressed here in the context of a single-compartment neuron model applying the ISO learning rule. We motivate

the use of this rule for modeling STDP by the fact that it is a differential Hebbian learning rule that correlates input and output signals and produces antisymmetrical weight change curves (Porr & Wörgötter, 2003a). On the right timescale, these properties are similar to STDP such that the ISO learning rule should in principle be applicable in this context too.

Currently it is generally assumed that backpropagating spikes provide the necessary postsynaptic signal that represents the temporal reference for the considered synapse. This view has recently been questioned (see Goldberg, Holthoff, & Yuste, 2002, for a review), and a stronger emphasis has been laid on local dendritic processes. Therefore, we will specifically investigate how different possible sources of postsynaptic depolarization, modeled by different shapes of the potential change, will influence learning. The central finding of this modeling exercise is that the ISO learning rule leads in a robust and generic way to STDP, while the shape of the input signals distinctively influences the shape of the weight change curve.

We believe that this study may help to further our understanding of more complex (compartmentalized or kinetic) models because the question of how a certain STDP curve arises is reduced to the question of how the cellular parameters lead to the underlying input signal shapes.

## 2 Methods

---

**2.1 Components of the Membrane Model.** The model represents a small, nonspiking, dendritic compartment with synaptic connections that can take the shape of an AMPA or an NMDA characteristic.

Thus, conductances  $g_A$  of AMPA and  $g_N$  of NMDA channels were modeled by state-variable equations:

$$g_i := g_A(t) = \bar{g}_A \hat{g}_A(t) = \bar{g}_A t e^{-t/t_{peak}} \quad (2.1)$$

$$g_i := g_N(t) = \bar{g}_N \hat{g}_N(t) = \bar{g}_N \frac{e^{-t/\tau_1} - e^{-t/\tau_2}}{1 + \eta[Mg^{2+}] e^{-\gamma V}}. \quad (2.2)$$

This slightly more complex notation is used because we will need the normalized conductance time functions  $\hat{g}_{A,N}(t)$  on their own when introducing the learning rule.

All equations used in this study are numerically evaluated in 0.1 ms time steps.

$V$  is the membrane potential. Peak conductances are given by the  $\bar{g}$  values:  $\bar{g}_A = 5.436$  nS/ms,  $\bar{g}_N = 4$  nS. The other parameters were  $t_{peak} = 0.5$  ms,  $\tau_1 = 40$  ms,  $\tau_2 = 0.33$  ms,  $\eta = 0.33$ /mM,  $[Mg^{2+}] = 1$  mM,  $\gamma = 0.06$ /mV (Koch, 1999). Reversal potentials used were  $E_A = E_N = 0$  mV.

The conventional membrane equation (equation 2.3) was used to determine the momentarily existing membrane potential:

$$C \frac{dV(t)}{dt} = \sum_i (\rho_i + \Delta\rho_i) g_i(t) (E_i - V(t)) + \frac{V_{rest} - V(t)}{R}, \quad (2.3)$$

with  $R = 100 \text{ M}\Omega$ ,  $C = 50 \text{ pF}$ , and  $V_{rest} = -70 \text{ mV}$  (Koch, 1999). Here we have introduced synaptic weights  $\rho_i$  and their weight changes  $\Delta\rho_i$ . This is done purely for convenience, because weights and peak conductances could also be combined multiplicatively. However, as we will see below, it makes sense to keep them separate, because the peak conductances  $\bar{g}$  can then serve as reference values for the growth (or shrinkage) of the synaptic weights. These equations were modeled using C++ in the Z-domain (Köhn & Wörgötter, 1998) in order to speed up simulations.

A single synapse was assumed as the so-called plastic synapse (PS) on which the influence of the ISO learning rule was tested. This synapse can consist of varying NMDA and AMPA components, and we will call it  $\rho_1$ . Note that only the NMDA component drives the learning (see below), the AMPA component will only (mildly) influence the membrane potential, thereby possibly exerting a second-order influence on the learning. It will, however, turn out in the course of this study that the secondary AMPA influence is so small that it can be neglected in most cases. The plastic synapse receives the presynaptic spikes modeled as  $\delta$ -function input to equations 2.1 and 2.2. The influence of the NMDA component of the plastic synapse on the membrane potential is dependent on the membrane's depolarization level. We assume in this model that this is determined by the postsynaptic activity, and we tested how different postsynaptic events influence the weight change curve. To this end, three cases will be discussed: a postsynaptic influence that takes the shape of (1) an AMPA response, (2) an NMDA response, and (3) a backpropagating spike (BP spike; see Figure 1A). We will call these influences the postsynaptic depolarization source (DS). Since we will treat these cases one by one, we can associate them with the same weight (i.e., amplitude factor)  $\rho_0$ . When using a BP spike, we have generally set  $\rho_0 = 1$ .

Technically this was achieved by triggering the depolarization source with another  $\delta$ -pulse that was shifted by a temporal interval  $T$  in relation to the presynaptic event. Physiologically this is meant to be linked to the postsynaptic spike. Strictly, this association, however, is valid only for the BP spike, which is causally related to the postsynaptic spike. The other (AMPA- or NMDA-) depolarization source events need not arise from such a causal relation but can be associated with other independently converging influences from other synapses. The possibility for neuronal synchronization (Singer & Gray, 1995) with different lead or lag supports the possibility that clusters of other synapses could lead to the required depolarization. At this point, we note that it is not possible to rigorously define  $T$  in all

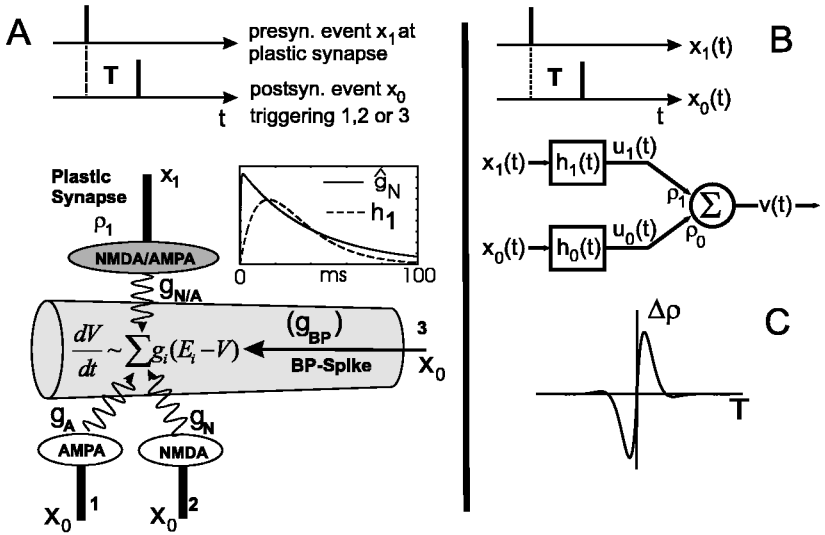


Figure 1: Schematic diagram of the model. (A) Components of the membrane model. The inset shows how to match the NMDA conductance function  $\hat{g}_N$  (see equation 2.2) with a resonator impulse response  $h_1$ . (B) Components of ISO learning. (C) Typical weight change curve obtained with ISO learning. Parameters to obtain this curve were  $Q = 0.51$ ,  $f = 0.1$  Hz.

instances. Experimentally,  $T$  is associated with the difference between pre- and postsynaptic spike. At the site of the plastic synapse, one would, however, expect a 1 to 2 ms larger  $T$  due to the delay in backpropagating the spike. If other clusters of synapses are driving the (heterosynaptic) plasticity,  $T$  would have to be defined as the interval between the cluster activity and that at the plastic synapse.

Figure 1A shows the different modeled depolarization sources in the context of a single-compartment model. At the summation point, the membrane potential is determined by the three depicted DS influences (see equations 2.1–2.3) as well as by the influence that comes from the plastic synapse. For practical purposes, we define  $T$  as the difference between the events as it occurs at the site of the plastic synapse, thus neglecting possible delays that are currently experimentally unresolvable.

One can assume that all active processes involved in generating BP spikes will cease at (or close to) the synaptic density. Thus, locally, only the electrotonic membrane properties will prevail. They are at the synaptic density determining the membrane potential, which in turn influences the state of the  $Mg^{2+}$  block at the NMDA channels and thus, the  $Ca^{2+}$  influx, which enters the CaMKII second messenger chain (Teyler & DiScenna, 1987). Therefore,

we have decided to model the BP spike also through a conductance change  $g_{BP}$  at the summation point (see equation 2.4), which mimics the physiologically measured shapes of BP spikes without having to implement active processes (active channels). Note that the actual equations used do not have any physiological meaning; they are used only to design realistic backpropagating spike shapes:

$$g_{BP}(t) = \bar{g}_{BP} \left( \frac{1}{1 + e^{-t/\tau_{rise}}} - \frac{0.5}{1 + e^{-(t-\tau_{BP})/\tau_{fall}}} - 0.5 \right). \quad (2.4)$$

With the help of this equation, rising ( $\tau_{rise}$ ) and falling flanks ( $\tau_{fall}$ ), as well as the total width ( $\tau_{BP}$ ) of our backpropagating spikes, can be adjusted independently, while their amplitude is controlled by  $\bar{g}_{BP}$ . This allowed us to design different shapes of backpropagating spikes in a very specific way.

BP spikes modeled according to equation 2.4 always have a typical shape. In order to cover transitory cases of a BP spike with a shape that is intermediate to the different shapes obtainable by equation 2.4, we used equation 2.5 (Krukowski & Miller, 2001):

$$g_{BP}(t) = \bar{g}_{BP} (f e^{-t/\tau_a} + (1 - f) e^{-t/\tau_b} - e^{-t/\tau_c}). \quad (2.5)$$

Actual parameters for equations 2.4 and 2.5 shall be given in the figure legends. To calculate the membrane potential, we assumed in all cases  $E_{BP} = 0$  mV.

A paired pulse protocol was used to stimulate the inputs. The pulse interval between both inputs (defined as  $T$ ) was varied between  $-50$  and  $+50$  ms. The interval between pulse pairs was  $\mathcal{T} = 250$  ms in order to prevent second-order interactions between pulse pairs (steady-state condition).

**2.2 Components of ISO Learning.** Figure 1B shows the circuit diagram of rate-based ISO-learning for only two ( $\delta$ -pulse) inputs  $x_0, x_1$  (for a more general description, see Porr & Wörgötter, 2003a). The inputs are first bandpass filtered by means of heavily damped resonators  $h$  defined by

$$h(t) = \frac{1}{b} e^{at} \sin(bt), \quad (2.6)$$

with  $a := -\pi f/Q$  and  $b := \sqrt{(2\pi f)^2 - a^2}$ , where  $f$  is the center frequency of the resonator and  $Q \geq 0.5$  the damping factor. Generally we used  $Q = 0.51$  (Porr & Wörgötter, 2003a), and this strong damping leads essentially to a low-pass behavior. Elsewhere, we have discussed that this would suffice for learning, while using the equations for bandpass filters renders several advantageous mathematical properties (Porr & Wörgötter, 2003a). However, in the context of this study, the “bandpass” filters used are really rather low-pass filters. Such a bandpass (low-pass) filtering takes place in a generic way

at almost all membrane processes, and this allows us to easily associate the abstract operations  $h$  to more realistic cellular operations below. The transformed inputs  $u_{0,1}$  converge onto the learning unit with weights  $\rho_{0,1}$ , and its output is given by

$$v(t) = \rho_0(t)u_0(t) + \rho_1(t)u_1(t) \text{ where } u_{0,1}(t) = x_{0,1}(t) * h(t). \quad (2.7)$$

The  $*$  denotes a convolution. In this study, we keep the weight  $\rho_0$  fixed. The other weight  $\rho_1$  changes by the ISO learning rule that uses the temporal derivative of the output:

$$\frac{d}{dt}\rho_1 = \mu u_1(t)v'(t) \quad \mu \ll 1. \quad (2.8)$$

In the original article, we had shown that ISO learning produces a linear weight change that can be calculated for all  $t \geq 0$  by solving

$$\rho_1 \rightarrow \rho_1 + \Delta\rho_1 \quad (2.9)$$

$$\Delta\rho_1(T) = \mu \int_0^\infty u_1(T + \tau)v'(\tau)d\tau. \quad (2.10)$$

This integral can be solved analytically and leads to the ISO learning weight change curve shown in Figure 1C for two identical bandpass filters  $h$ . Note that this curve becomes skewed if two different bandpass filters are used, which indicates that the shapes of the input functions  $u$  are critical in determining the shape of the weight change curve.

**2.3 Associating the Membrane Model to ISO Learning.** We need to associate the parameters of the ISO learning rule with those in the membrane model for the plastic synapse  $\rho_1$ :

- $x_1$ : We assume that the presynaptic spike train at the plastic synapse represents the signal  $x_1$  of ISO learning.
- $h_1$ : The bandpass filter operation  $h_1$  is represented by the conductance functions  $g$  of the plastic synapse, and we define

$$h_1(t) := \hat{g}_N(t). \quad (2.11)$$

- $u_1$ : Since we are only dealing with spike trains modeled as  $\delta$ -functions, we get  $u_1(t) = h_1(t) = \hat{g}_N(t)$ . Corresponding curves are shown in the inset of Figure 1A. This shows that the conductance function essentially captures the characteristic of low-pass filtering the spike at the input. The match between the curves, however, is not exact, immediately indicating that the results of the membrane model will not be identical to those of ISO learning.

- $v$ : The membrane potential  $V$  is associated straightforwardly to the output function  $v$  from ISO learning. Note, as opposed to the original linear ISO learning rule, that we observe that the biophysically adapted version introduced here is no longer linear. The results presented later, however, will show that the adapted rule will still lead to generic antisymmetrical weight change curves. The nonlinearities introduced by the reversal potentials, as well as by the voltage dependence of the NMDA channel, influence the results only qualitatively.
- $x_0$ : The signal  $x_0$  from ISO learning is associated with three possible signals: with a spike arriving at input 1 (AMPA) or 2 (NMDA) or with a BP spike (see equation 2.3) in Figure 1A.
- $u_0$ : It is not necessary to associate  $u_0$  with any component of the membrane model because it does not influence the plastic synapse  $\rho_1$  directly. Instead, this happens only via the derivative of the membrane potential.<sup>1</sup> Essentially  $u_0$  represents the conductance change for any of the three introduced depolarization sources (see equations 2.1–2.3 and Figure 1A).
- $\rho_{0,1}$ : Synaptic weights had been directly introduced into the membrane equation (see equation 2.3).  $\rho_1$  is the initial value of the synaptic weight of the plastic synapse.  $\rho_0$  is used as the amplitude factor for a possible second synapse or the BP spike. Thus,  $\rho_0$  defines the strength of the depolarization source.
- *Learning rule*: As a consequence of these settings, the learning rule of ISO learning is rephrased in the context of this model to

$$\frac{d}{dt}\rho_1 = \mu u_1(t)v'(t) = \mu \hat{g}_N(t) V'(t). \quad (2.12)$$

In section 4, we will address the question of the physiological relevance of the different parts of this learning rule and show how to associate pre- and postsynaptic events with the different terms. Here we only note that this rule in its derivative form can be associated to calcium flow through NMDA channels or in its integrated form to the calcium concentration (see section 4).

Note that this rule is (as usual) treated in an adiabatic condition assuming that multiple spike pairs (with interspike interval  $T$ ), which occur with a temporal distance of  $\mathcal{T}$  between them, do not influence each other. Thus, for the actual weight change  $\Delta\rho$  obtained with one

---

<sup>1</sup> In a symmetrical learning situation (with  $\rho_0$  changing also), one could associate  $u_0$  with the corresponding conductances  $\hat{g}$  in a similar way as for  $u_1$ .

spike pair at the inputs, we use equation 2.10 and calculate

$$\Delta\rho_1 = \int_0^t \frac{d\rho_1}{dt} dt, \quad (2.13)$$

where  $T \ll t \ll T$ . We call  $\Delta\rho$  an integrated weight change.

The learning rate  $\mu$  takes the unit of  $\text{Volt}^{-1}$ , because this way  $\Delta\rho$  is rendered unit free. To regard  $\mu$  as a voltage-dependent entity may make sense given the observation that predepolarization enhances the induction of LTP and vice versa (Sourdet & Debanne, 1999).

The physiological meaning behind the concept of a synaptic weight is still under debate. Several pre- and postsynaptic mechanisms contribute to the weight (Malenka & Nicoll, 1999), which in this study are subsumed under a single number  $\rho$ . However, using these settings,  $\rho$  can be treated as a multiplicative factor of the peak conductance  $\bar{g}$ , which, multiplied together, can be interpreted as the strength of a given connection in the context of this model. At this point, it is important to note that the final value of  $\mu$  is rather arbitrary, because it is just a multiplicative factor that changes the slope of the (linear, see below) learning curve. In physiology, there exist (intracellular) amplification mechanisms that could in principle be associated with such a  $\mu$ -factor. This does not make sense in the context of this model because such mechanisms are not implemented. Thus, we will set the value of  $\mu = 1$  and provide an analysis about the range of  $\mu$  within which the model operates linearly (see Figure 7).

### 3 Results

---

In this section, we present results obtained when using a pure NMDA-synapse as the plastic synapse. At the end of this section, we discuss the physiologically more realistic case of a mixed AMPA/NMDA synapse, showing how to infer the corresponding results from what we have presented before. We use the three different sources for a postsynaptic depolarization introduced in section 2: a BP spike (**3** in Figure 1A), which is currently believed to be the most likely source of depolarization, but also a pure AMPA influence (see **1** in Figure 1A) or a pure NMDA influence (see **2** Figure 1A). The goal of this section is to distinguish unrealistic from more realistic cases and to arrive at some conclusions concerning the robustness of the obtained results.

In all the cases, we set the relative initial strength of the plastic synapse to  $\rho_1 = 0.5$ , which means that the synaptic weight of this connection was initially at  $0.5\bar{g}_N$ . The weight  $\rho_0$ , usually set to 1, is kept constant.

**3.1 Individual Weight Change Examples.** Figure 2A shows the conductance  $g_N$ , Figure 2B the membrane potential and Figure 2C its derivative,

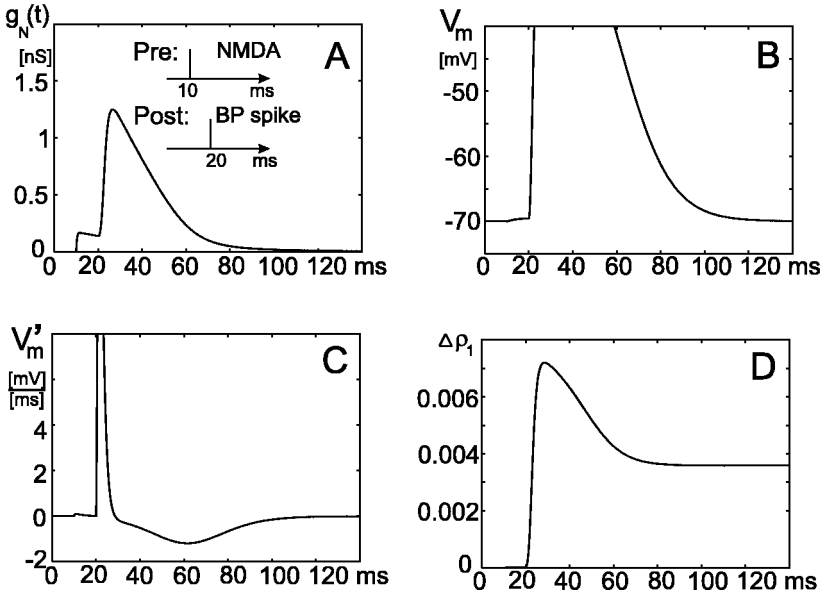


Figure 2: Detailed curves for a single pulse pair experiment with  $T = 10$  ms and a BP spike as the depolarization source,  $\rho_0 = 1$ . (A) Conductance change  $g_N$  arising from the presynaptic input and as a consequence of the BP spike leading to positive feedback at the  $e^{-\gamma V}$ -term in equation 2.2. (B) Membrane potential change. (C) Derivative of the membrane potential. (D) Resulting integrated weight change. The weight stabilizes as soon as all curves have returned to their equilibrium.

and Figure 2D the development of the plastic synapse  $\rho_1$  for a single input pulse pair with the first spike arriving at  $t = 10$  ms at the plastic synapse (presynaptic spike) and the BP spike arriving at  $t = 20$  ms. Thus, we have a positive value for  $T = +10$  ms. The initial membrane potential was at resting level ( $-70$  mV) for this simulation. The plastic synapse was assumed to be a pure NMDA synapse.

The small increase in the NMDA conductance  $g_N$  (see Figure 2A) starting at  $t = 10$  ms is caused by a spike at the plastic synapse. The following large peak is due to the rising membrane potential as soon as the BP spike arrives at 20 ms. The membrane potential (see Figure 2B) increases slightly at  $t = 10$  ms because of the activated NMDA channel and is dominated by a BP spike later. The upper part of the membrane potential curve (see Figure 2B) is not shown in order to make the small NMDA channel response more visible.

An integrated weight change  $\Delta\rho_1$  (see Figure 2D) occurs throughout the duration of the membrane potential excursion. It follows the rule given in

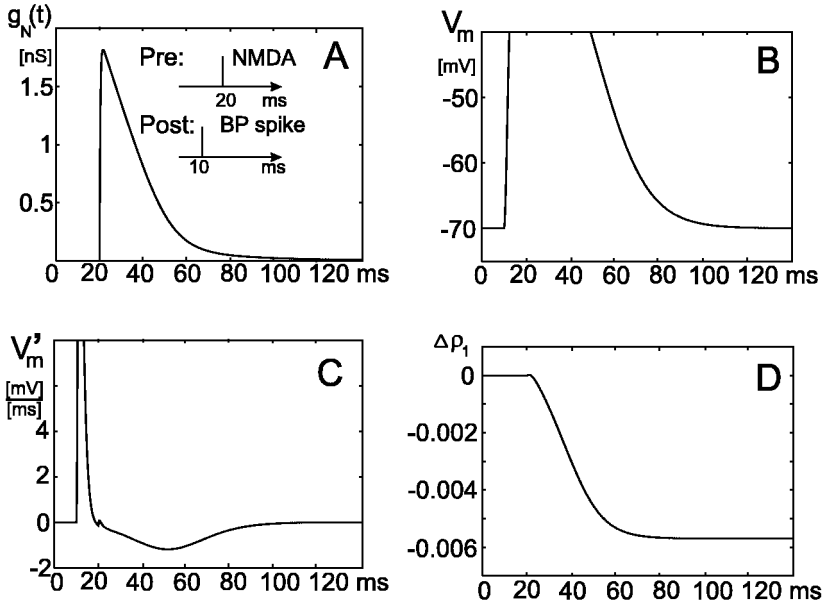


Figure 3: Detailed curves for a single pulse pair experiment with  $T = -10$  ms. Panels are the same of those in Figure 2, only in this case, a negative integrated weight change is obtained (D).

equation 2.12 integrated according to equation 2.13, and the weight finally stabilizes slightly above zero as soon as the membrane potential returns to resting. The obtained change is small because only a single pulse pair was used.

Essentially, the opposite situation is observed when inverting the pulse sequence to  $T = -10$  ms (see Figure 3). The negative excursion of the derivative of the membrane potential (C) is now scaled with the full  $g_N$  influence (A), leading to a strong drop of the integral and finally to a reduced weight  $\rho_1$  at steady state (D).

Figure 4A shows complete weight change curves obtained at different resting potentials  $V_{rest} = -40$  to  $-70$  mV. We observe that the shape of the curves remains essentially the same while the magnitude of the weight change grows slightly when the membrane potential is depolarized. This is in accordance with observations that the amplitude of LTP can be augmented by prepolarizing the cell under study as a consequence of the voltage dependence of the NMDA channel (Sourdet & Debanne, 1999). Part B of Figure 4 has been obtained with a second synapse as the depolarization source and shall be discussed later.

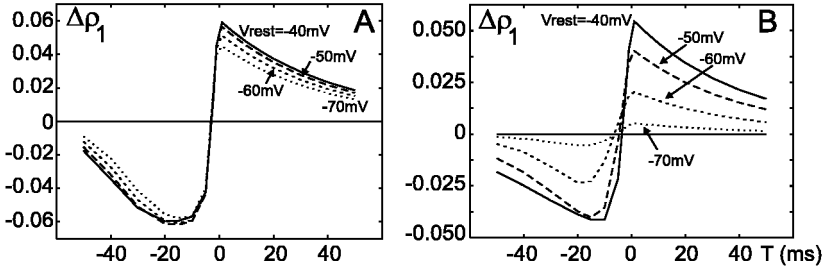
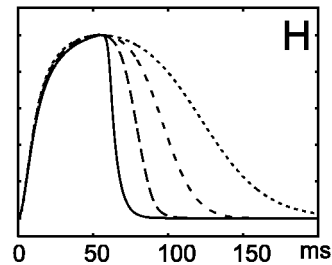
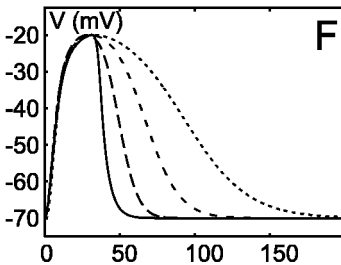
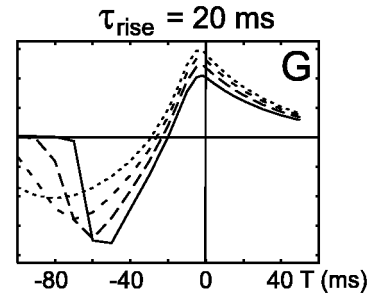
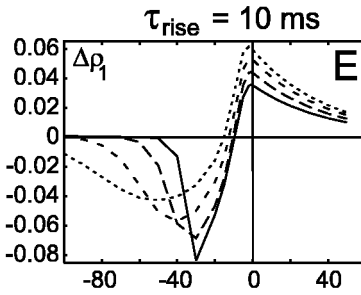
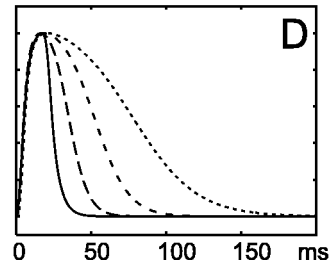
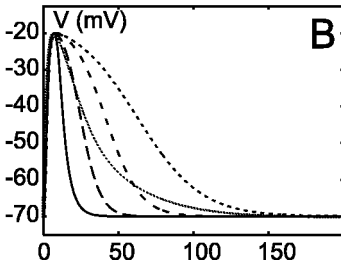
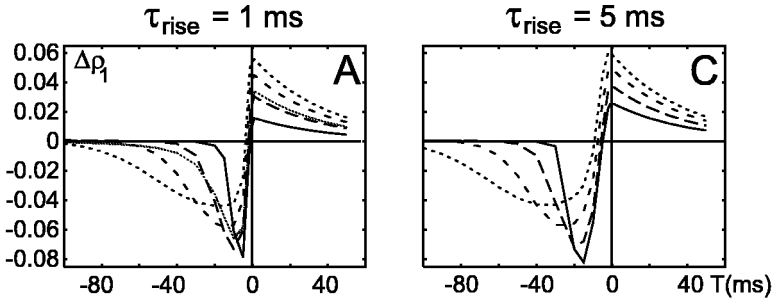


Figure 4: Weight change curves obtained at different resting potentials. (A) Using a BP spike as depolarization source. The BP spike is modeled with equation 2.4 and parameters  $\tau_{rise} = 1$  ms,  $\tau_{fall} = 10$  ms,  $\tau_{BP} = 25$  ms,  $\bar{g}_{BP} = 59.8$  nS,  $\rho_0 = 1$ . (B) Using a second NMDA synapse as the depolarization source,  $\rho_0 = 10$ .

**3.2 Influence of the Shape of the BP Spike.** Figure 5 shows 17 weight change curves and the BP spikes with which they were obtained. Note that some of these spike shapes do not necessarily reflect realistic BP spike shapes. Instead, this modeling exercise is meant to cover a rather complete range of composable shapes such that the characteristics of a weight change curve resulting from any other BP spike shape can be inferred from this diagram. In general, we observe that the negative part of the weight change curve dominates in most cases across all panels, which is in accordance with physiology (Debanne, Gahwiler, & Thompson, 1998; Feldman, 2000).

Figure 5: *Facing page.* Weight change curves obtained with different BP spikes as the depolarization source. Top panels show the weight change curves and bottom panels the BP spikes with which they were obtained. BP spikes were modeled using equation 2.4, adjusted to the same amplitude. A and B also contain one example obtained with a BP spike with intermediate shape modeled with equation 2.5. This spike starts with the shape of the first BP spike in B and ends with the shape of the last spike. In all cases we used  $\rho_0 = 1$ . Individual parameters for the different BP spikes were: A, B:  $\tau_{rise} = 1$  ms: ( $\tau_{fall} = 1$  ms,  $\tau_{BP} = 9$  ms,  $\bar{g}_{BP} = 56$  nS); ( $\tau_{fall} = 5$  ms,  $\tau_{BP} = 15$  ms,  $\bar{g}_{BP} = 61.4$  nS); ( $\tau_{fall} = 10$  ms,  $\tau_{BP} = 25$  ms,  $\bar{g}_{BP} = 59.8$  nS); ( $\tau_{fall} = 20$  ms,  $\tau_{BP} = 30$  ms,  $\bar{g}_{BP} = 67.5$  nS). C, D,  $\tau_{rise} = 5$  ms: ( $\tau_{fall} = 1$  ms,  $\tau_{BP} = 20$  ms,  $\bar{g}_{BP} = 56$  nS); ( $\tau_{fall} = 5$  ms,  $\tau_{BP} = 25$  ms,  $\bar{g}_{BP} = 64$  nS); ( $\tau_{fall} = 10$  ms,  $\tau_{BP} = 35$  ms,  $\bar{g}_{BP} = 63$  nS); ( $\tau_{fall} = 20$  ms,  $\tau_{BP} = 45$  ms,  $\bar{g}_{BP} = 67.5$  nS). E, F,  $\tau_{rise} = 10$  ms: ( $\tau_{fall} = 1$  ms,  $\tau_{BP} = 35$  ms,  $\bar{g}_{BP} = 56$  nS); ( $\tau_{fall} = 5$  ms,  $\tau_{BP} = 40$  ms,  $\bar{g}_{BP} = 62$  nS); ( $\tau_{fall} = 10$  ms,  $\tau_{BP} = 50$  ms,  $\bar{g}_{BP} = 63.5$  nS); ( $\tau_{fall} = 20$  ms,  $\tau_{BP} = 60$  ms,  $\bar{g}_{BP} = 69$  nS). G, H,  $\tau_{rise} = 20$  ms, ( $\tau_{fall} = 1$  ms,  $\tau_{BP} = 60$  ms,  $\bar{g}_{BP} = 57.5$  nS); ( $\tau_{fall} = 5$  ms,  $\tau_{BP} = 70$  ms,  $\bar{g}_{BP} = 60$  nS); ( $\tau_{fall} = 10$  ms,  $\tau_{BP} = 80$  ms,  $\bar{g}_{BP} = 62$  nS); ( $\tau_{fall} = 20$  ms,  $\tau_{BP} = 90$  ms,  $\bar{g}_{BP} = 68$  nS). Parameters for the BP spike with intermediate shape in A and B are  $\tau_a = 7$  ms,  $\tau_b = 30$  ms,  $\tau_c = 4$  ms,  $f = 0.9$ ,  $\bar{g}_{BP} = 10.9$  nS.



$\tau_{\text{fall}}$ : — 1 ms -- 5 ms - - - 10 ms ..... 20 ms  
 Intermed. shape in panels A,B only —

By comparing the curves within each panel, it can be seen that increasing fall times ( $\tau_{fall}$ ) of the BP spike mainly lead to an increase of the positive peak of the weight change curve, while the negative peak becomes smaller but more spread out toward negative values of  $T$ .

By comparing curves across panels, one can assess the influence of increasing rise times ( $\tau_{rise}$ ). Here we observe that the typical STDP shape of the curves in Figure 5A (zero crossing at about  $T = 0$  ms) becomes similar to standard Hebbian learning for values of  $T > -20$  ms for a rather shallow rise time  $\tau_{rise} = 20$  ms of the BP spikes in Figure 5G. Only for  $T < -20$  ms are negative weight changes again obtained. This effect becomes more pronounced when increasing the rise times to values  $\tau_{rise} > 20$  ms. Such shallow rise times may indeed occur at distal dendrites where, discounting possible active processes, the membrane capacitance has smeared out a BP spike substantially (Magee & Johnston, 1997; Larkum, Zhu, & Sakmann, 2001). When cells are driven, for example, by a stimulus, pre- and postsynaptic spikes will follow each other, often in intervals of less than 20 ms (Froemke & Dan, 2002). Thus, the values of a weight change curve for  $T$  beyond  $\pm 20$  ms are probably many times not of relevance for a cell's synaptic plasticity (Froemke & Dan, 2002). Therefore, the shape-dependent leftward shift of the weight change curve leading to LTP within rather larger temporal intervals could be of some theoretical interest, because it shows that we do not have to alter the learning rule in order to get either differential Hebbian learning or a characteristic that is similar to standard Hebbian learning at realistic interspike intervals. A changing input characteristic will do the trick already.

Note that in general, the plastic NMDA synapse will contribute almost nothing to the membrane potential change as compared to the strong influence of the BP spike. Thus, in the specific case of Figures 5G and 5H, the derivative of the membrane potential will remain positive for rather long durations as soon as the rise time is large. This leads to positive weight changes also for large negative  $T$  values.

The one example of a BP spike with intermediate shape (see Figures 5A and 5B) shows, and quite expectedly so, that gradual spike shape transitions will also lead to gradual transitions of the shape of the weight change curves. This supports the notion that other shapes of weight change curves can be basically inferred from these examples.

**3.3 Influence of Different NMDA Characteristics.** It is known that during development, the relative frequency of different NMDA receptor types (NMDAR<sub>A</sub> versus NMDAR<sub>B</sub>) changes. This influences the electrophysiological properties of the NMDA channel. Figures 6A and 6B show three different NMDA characteristics, the steepest reflecting an adult stage. The other two stages are observed during development at postnatal days 26 to 29 ( $\tau_{decay} = 380$  ms) and 37 to 38 ( $\tau_{decay} = 189$  ms) in ferret at a +40 mV voltage

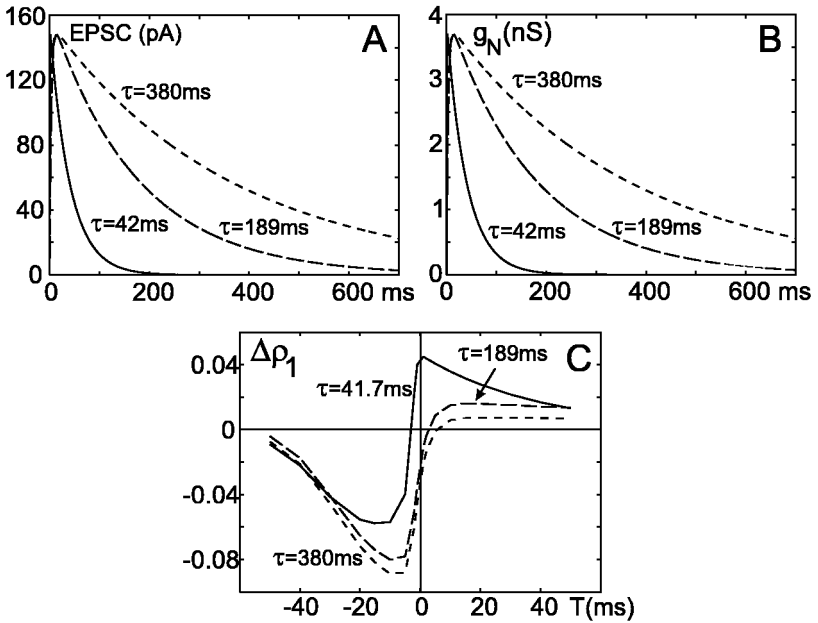


Figure 6: Learning curves obtained with different NMDA characteristics. (A) EPSC, (B) conductance of the NMDA synapse, both at +40 mV voltage clamp. (C) Weight change curves. Parameters for equation 2.2 were as follows. Normal (adult) NMDA:  $\bar{g}_N = 4$  nS,  $\tau_1 = 40$  ms,  $\tau_2 = 0.33$  ms which gives an EPSC with  $\tau_{decay} = 41.7$  ms. Young NMDA, before eye opening (26–29 days):  $\bar{g}_N = 4.02$  nS,  $\tau_1 = 363.1$  ms,  $\tau_2 = 0.033$  ms which gives EPSC with  $\tau_{decay} = 380$  ms. Older NMDA, after eye opening (37–38 days):  $\bar{g}_N = 4.2$  nS,  $\tau_1 = 173.3$  ms,  $\tau_2 = 0.033$  ms which gives EPSC with  $\tau_{decay} = 189$  ms. The BP spike was modeled according to equation 2.4 with parameters  $\tau_{rise} = 1$  ms,  $\tau_{fall} = 10$  ms,  $\tau_{BP} = 2.5$  ms,  $\bar{g}_{BP} = 59.8$  nS,  $\rho_0 = 1$ .

clamp preparation, where there is no more  $Mg^{2+}$  blockage of the NMDA channel. The single decay values for  $\tau_{decay}$  were taken from Roberts and Ramoa (1999), but we still modeled the NMDA characteristic using equation 2.2 by fitting our two  $\tau$ -values to yield the curves reported by Roberts and Ramoa. To obtain the weight change curves, we used a BP spike with a short rise time (1 ms) and a medium fall time (10 ms; compare Figure 5B). Interestingly we observe that both “young” NMDA synapses yield rather asymmetrical weight change curves with a strongly dominated LTD part. To our knowledge, so far very little is known about the actual physiological learning characteristics of early synapses. There are, however, indications that synaptic elimination dominates the early developmental stages (analyzed in a theoretical study by Chechik, Meilijson, & Ruppim, 1998). The

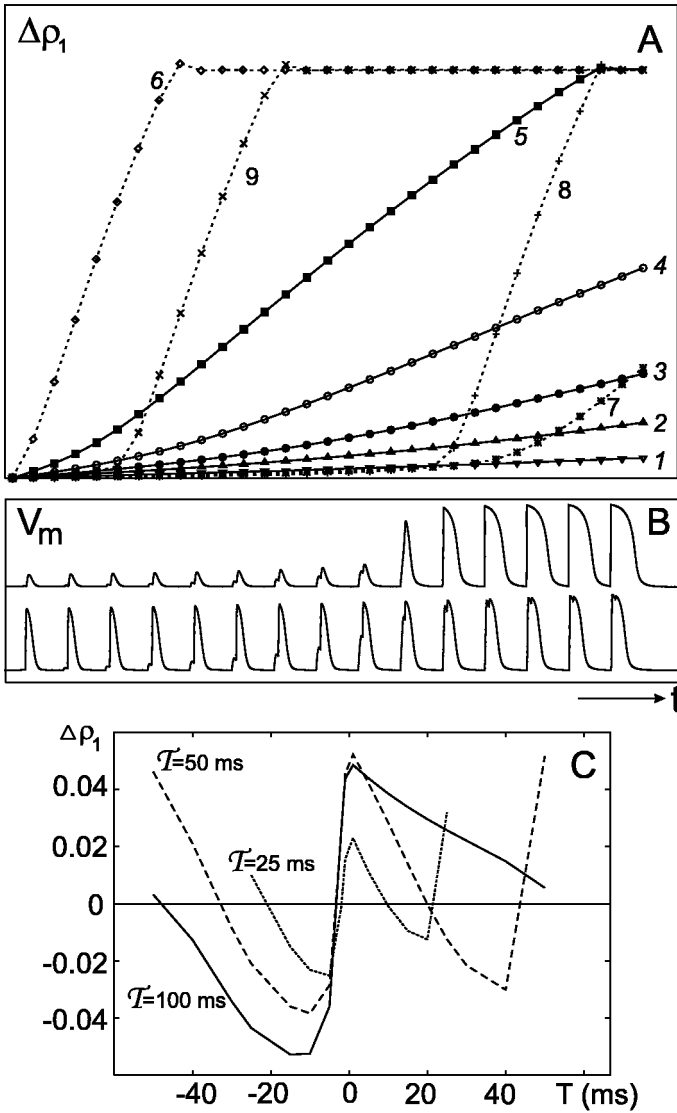
theoretical results obtained with our learning rule would possibly point toward this direction.

**3.4 Multiple Spike Pairs.** Figures 7A and 7B show how weights develop when using a sequence of 30 pulse pairs with interpair intervals of  $T = 100$  ms, which still guarantees the adiabatic condition for interspike intervals below  $T \pm 50$  ms (see Figure 7C). Different learning rates  $\mu \geq 100$  and varying amplitudes of the BP spike were applied to obtain Figures 7A and 7B. These high learning rates were used in order to be able to use only a few pulse pairs for measuring the whole curve. We find two different types of behavior. Curves 1 to 6 show a gradual increase with almost unchanging slope (until saturation, curves 5 and 6); curves 7 to 9 show weak growth until a certain point, from which they grow much faster. Curves with gradual, unchanging growth (1–6) are obtained as soon as the amplitude of the BP spike is large. To obtain them, we have kept the same BP spike amplitude and increased the learning rate. This way, weight growth can be adjusted to different values to match it to the physiologically obtained percentage weight changes if desired (Bi & Poo, 2001). Curves 7 to 9 were obtained with (very) small amplitudes of the BP spike. We observe that the left part of the curves still shows a very shallow increase, followed by a kink (or bend), which continues into a second steeper part of the curve followed by saturation in curves 8 and 9.

These differences can be explained by looking at how the membrane potential develops over time for the two different cases as shown in Figure 7B. Each depolarization represents the response of the model to a pulse pair ( $T = 25$  ms). Most of the time, two peaks are seen in the potential; the

---

Figure 7: *Facing page.* (A) Progress of the weight growth for a plastic NMDA synapse with initial value  $\rho_1 = 0.5$  and BP spikes of different amplitudes. We used  $T = 5$  ms as the temporal interval between pulses. Different slopes of the curves were obtained with different learning rates  $\mu$ , which were for curves 1–6 increasing as  $\mu = 100, 200, 300, 500, 1000, 3400$ , curve 7,  $\mu = 1000$ , curves 8 and 9,  $\mu = 3400$ . The BP spike was modeled according to equation 2.4 for all curves with parameters,  $\rho_0 = 1$ ,  $\tau_{rise} = 1$  ms,  $\tau_{fall} = 10$  ms,  $\tau_{BP} = 25$  ms; for curves 1–6,  $\bar{g}_{BP} = 59.8$  nS; for curves 7 and 9,  $\bar{g}_{BP} = 4$  nS; for curve 8,  $\bar{g}_{BP} = 0.4$  nS. The resulting BP spike amplitude  $V_{max}$  was for curves 1–6  $V_{max} = -20$  mV, curves 7 and 9  $V_{max} = -61$  mV, curve 8,  $V_{max} = -69$  mV. Interpair interval  $T = 100$  ms. (B) Membrane potential traces comparing the cases with and without steep increase. Here we used  $T = 25$  ms to make the individual contributions of both pulses more visible. The top panel corresponds to curve 9, the bottom panel to curve 3. Interpair interval  $T = 100$  ms. (C) Weight change curves obtained with multiple spike pairs at different interpair intervals  $T = 100, 50, 25$  ms. Parameters were:  $\mu = 1$ ,  $\rho_0 = 1$ ,  $\tau_{rise} = 1$  ms,  $\tau_{fall} = 10$  ms,  $\tau_{BP} = 25$  ms,  $\bar{g}_{BP} = 59.8$  nS.



first comes from the plastic synapse and the second from the BP spike. The bottom trace represents a case where the amplitude of the BP spike was relatively large (as for curves 1–6). As a consequence, the general shape of the potential is very strongly dominated by the BP spike; the plastic synapse does not contribute much to it. In the top trace, we have used a very small BP spike amplitude (as for curves 7–9). This time, the potential is dominated

by the growing plastic synapse. Given that this is a pure NMDA synapse, we obtain positive feedback through the  $e^{-\gamma V}$  term in equation 2.2. Hence, we get a very steep increase as soon as this synapse gets “overly” strong. As a result, we get a slope in curves 8 and 9 that is the same as that in curve 6, which was obtained by a large BP spike and the same high learning rate ( $\mu = 3400$ ). For the same reason, the slopes of curves 5 and 7 at the right side of the diagram are also similar. Note that if we use the small learning rate of  $\mu = 1$  that we normally applied, we still expect the same basic behavior but only after many more input pairs and with a much shallower nonlinear increase as soon as the positive feedback sets in.

It is not conceivable that the situation shown in curves 7 to 9 directly corresponds to physiology, because one rarely finds pure NMDA synapses that at the same time would have to grow very strongly before being able to elicit this effect. However, a cluster of mixed AMPA and NMDA plastic synapses at the peripheral dendrite (or at a spine) where the BP spike might be small could indeed lead to local nonlinear potential changes resulting in such effects.

Figure 7C shows weight change curves obtained with different interpair intervals  $\mathcal{T}$ , as indicated in the figure. This shows that the adiabatic condition is violated as soon as interspike intervals  $T$  approach the interpair interval. As a consequence, secondary LTP (or LTD) regions appear as expected from the results of Froemke and Dan (2002). Bi (2002) discusses various cases of spike pair combinations that could lead to such results; explicit experimental proof of this model prediction, however, is at the moment still lacking.

**3.5 Weight Change Curves Obtained with a Second Synapse as Depolarization Source.** It is known that the postsynaptic depolarization signal is needed in order to remove the  $\text{Mg}^{2+}$  block at the NMDA channels, without which no  $\text{Ca}^{2+}$  could enter the cell. A BP spike provides a very strong source of depolarization. More locally, however, other sources of postsynaptic depolarization also can exist, especially when considering clusters of synapses. Here “any other” synapse could lead to a local depolarization affecting the plastic NMDA synapse under consideration. This would lead to heterosynaptic plasticity, and Goldberg, Staff, and Spurston (2002) discuss the biophysical implications of this alternative.

Accordingly, Figure 8 shows two groups of curves obtained with a plastic NMDA synapse and different synaptic depolarization sources. Depolarization comes from a cluster of AMPA synapses for A curves and a cluster of NMDA synapses for B curves. Both types of curves, A and B, are antisymmetrical, but the generic shape differs. Curves A have a skewed asymmetry and a slight positive offset, while curves B possess almost equal LTD and LTP parts and are shifted above zero for weak depolarization.

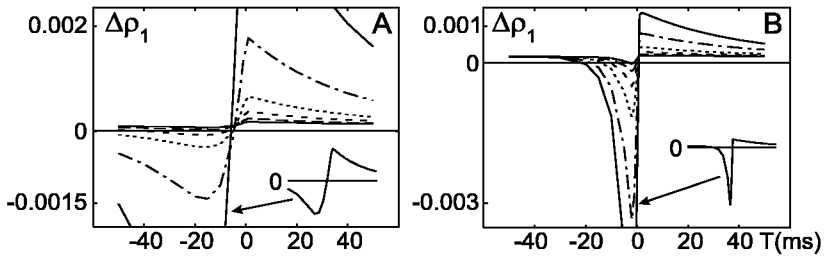


Figure 8: Weight change curves obtained with differently strong depolarization source amplitudes  $\rho_0$ . In general, an increase in depolarization source amplitude leads to an increase of the amplitude of the weight change curves. Insets show the shape of the two cut-off curves pointed to with the arrows at a reduced magnification. (A) Using an NMDA synapse as the depolarization source with  $\rho_0 = 0.25; 0.5; 1; 2; 5; 10$ . (B) Using an AMPA synapse with  $\rho_0 = 0.25; 0.5; 1; 2; 5; 10$ .

Nothing is known about STDP at synaptic clusters, and our results show that plasticity may have a different form when depolarization is caused by synchronized synapses and not a BP spike.

The different curves in Figures 8A and 8B are obtained setting  $\rho_0$  between 0.25 and 10 and thus assuming different relative strengths of the depolarization source.<sup>2</sup>

In all cases, we observed that the strength of the depolarization source acts as an amplification factor, leaving the shape of the curves essentially unchanged. As noted above, pure amplification is meaningless in the context of these simulations because this can be achieved by a changed learning rate  $\mu$  or a larger number of paired pulses as well. Interestingly, we found that a changing depolarization source strength not only affects amplification but also induces a shift of the curves with respect to zero. The smallest curves, which were obtained with a weak depolarization source, remain above zero all the time. Thus, in spite of their realistic looking shape, these curves do not represent STDP. For larger values of DS ( $\rho_0 \geq 0.5$ ), a zero crossing is observed, and only for the largest curve (DS:  $\rho_0 = 10$ ), the negative part covers more area than the positive part, which seems to be the generic case for most STDP curves.

Furthermore, weight changes are about tenfold smaller as compared to the cases above, where we had used a BP spike as the depolarization source

<sup>2</sup> In principle, it would be possible to keep the relative strength of DS equal to 0.5 and vary the strength of PS. This, however, is essentially symmetrical to the experiments shown, because only the quotient between the strength of PS and DS determines the shape of the resulting STDP curves. This holds apart from minor effects due to the recurrent influence of the NMDA channel.

(except for the cases  $\rho_0 = 10$ ). This is due to the much stronger change in membrane potential arising from a BP spike. As a consequence, a tonic depolarization of the membrane potential will lead to a stronger amplification of the weight change curves when using a second synapse as depolarization source (see Figure 4B) as compared to the situation where we had used a BP spike.

**3.6 Mixed NMDA/AMPA Plastic Synapses.** So far we have looked only at pure NMDA synapses as the plastic synapse. This is not in accordance with physiology because most synapses, which contain NMDA components, are mixed NMDA and AMPA synapses (as depicted in Figure 1A), moreover normally with a dominating AMPA part (Malenka & Nicoll, 1999). In addition, one finds that during learning, the AMPA component of such synapses undergoes much stronger changes than the NMDA component (Lüscher & Frerking, 2001; Song & Hugarir, 2002). This happens in spite of the fact that it is the NMDA component that is the driving force of the learning. This last observation, however, justifies formulating the learning rule used here by only the normalized NMDA conductance function  $\hat{g}_N$  in equations 2.11 and 2.12. Thus, the AMPA component cannot directly enter learning at equation 2.12; it will, however, influence the membrane potential  $V$  and thereby exert two effects: (1) it influences the  $e^{-\gamma V}$  term in the NMDA conductance function (see equation 2.2) and (2) it influences directly the derivative of the membrane potential. Both effects could change learning.

However, at this stage of the analysis, we have arrived at the conclusion that the BP spike is in most cases the strongest and most influential depolarization source, which is in accordance with others (reviewed in Linden, 1999, but see Goldberg et al., 2002). Above, we have argued that the depolarization that comes from a BP spike is normally much stronger than that which occurs from the plastic synapse itself that the influence of the plastic synapse on the membrane potential can be neglected. This still holds for mixed AMPA and NMDA synapses. A realistic single excitatory postsynaptic spike potential (EPSP) is normally rather small. Thus, as long as the BP spike is still strong, a single EPSP will not substantially influence learning. As soon as the BP spike drops in amplitude, one would have to consider the effect of a mixed plastic synapse. In this case, the learning curve will gradually approach the shape shown in Figure 8B, where we have a pure AMPA component assumed as the depolarization source and we will get nonlinear learning behavior such as that observed in Figure 7, curves 7 to 9. The wide range of possible effects that might arise from this, however, exceeds the scope of this article.

## 4 Discussion

---

This study consists essentially of two parts. The first part is the association between the ISO learning model and its biophysical counterpart, and the

second part concerns the actual findings obtained from the new model. We discuss both parts consecutively. At the end of this section, we compare our model to others found in the literature.

**4.1 Discussing the Model Assumptions.** ISO learning is a typical artificial neural network algorithm, and it is therefore rather unrelated to biophysics. As a consequence, any kind of biophysical reevaluation cannot immediately go all the way down toward individual channel and calcium dynamics. Instead, in this study we have attempted to go one step into this direction by adapting the ISO learning algorithm to a traditional state-variable description of a neuronal (compartmental) model. One central assumption of ISO learning is the filtering of its inputs. In a neuron, low-pass filtering takes place in a very natural way as the consequence of the NMDA channel properties, as well as from the low-pass characteristics of natural membranes. Obviously these low-pass filters are not identical to the technical bandpass filters used in ISO learning, but deviations are small enough in order to yield the same basic STDP-like learning behavior.

ISO learning was designed to correlate two inputs with each other in time (e.g., in a temporal sequence learning paradigm). STDP, however, takes place in relation to the temporal structure between a neuron's input (presynaptic) and its output (postsynaptic). In spite of this apparently different algorithmic structure, adaptation of both models is still straightforward when realizing that normally a postsynaptic spike has been elicited from some presynaptic influence. This justifies our approach of either assuming a second (cluster of) synchronized synapse(s), a dendritic spike, or a BP spike as a possible depolarization source (Linden, 1999; Goldberg et al., 2002).

The learning rule consists of two components. The second term is given by the derivative of the membrane potential. In most cases, the membrane potential is strongly dominated by the shape of the BP spike at the moment of pairing, while the contribution of the plastic synapse (or other synapses) can be neglected. This makes  $V'$  a postsynaptic quantity. Given that  $V' = \frac{1}{C}$ , we note that the learning rule can be rewritten also as  $\frac{d\rho}{dt} = \frac{\mu}{C} \hat{g} \frac{dQ}{dt}$ . This shows that charge transfer  $\frac{dQ}{dt}$  across the (postsynaptic) membrane is a major driving force of learning.

We can assume that a part of  $\frac{dQ}{dt}$  is contributed by calcium flow (Malenka & Nicoll, 1999). Then after integration, the final weight change  $\Delta\rho$  is determined by part of  $Q$ , the total amount of calcium ions that crossed the membrane. This interpretation is valid as long as the calcium contributes an approximately fixed part to the total current. The model does not take into account more complex calcium dynamics, buffering, enzymatic reactions, or others that take place during physiological weight changes. This was clearly not intended at this level of model complexity.

As the first term of the learning rule, we have used the normalized NMDA conductance function  $\hat{g}_N$ , which represents the bandpass filtered input  $u_1$

of ISO learning's response to a  $\delta$ -pulse input. We would argue that  $\hat{g}_N$  essentially subsumes the time course of all processes that occur for an NMDA receptor outside or directly at the membrane—thus, all presynaptic events, for example, glutamate release, binding to the receptors, unbinding, and elimination from the synaptic cleft. The efficiency with which this happens is encoded in the scaling factor  $\bar{g}_N$ .

Thus, our learning rule uses a product of a presynaptic ( $\hat{g}$ ) and a postsynaptic ( $V'$ ) influence. From this, it is now clear that the association of  $V'$  with calcium flow must be restricted to that proportion of the calcium that travels through the NMDA channels. Voltage-gated calcium channels, calcium-induced calcium release, or other calcium buffer release mechanisms are not being considered in this model, which could potentially influence synaptic changes. There is, however, wide-ranging support (especially for spines) that synaptic plasticity is indeed strongly dominated by calcium transfer through NMDA channels (Schiller, Schiller, & Clapham, 1998; Yuste, Majewska, Cash, & Denk, 1999; Malenka & Nicoll, 1999) and that the other calcium release mechanisms may play only a minor role (but see, e.g., Huemmeke, Eysel, & Mittmann, 2002).

Note that in this study, we do not implement any mechanisms of short-term plasticity (Markram & Tsodyks, 1996; Fortune & Rose, 2001). In principle, this could be done using a fast model for short term plasticity (Giugliano, Bove, & Grattarola, 1999) as a front end that continuously adjusts the base value of  $\rho$  as soon as an input spike train arrives. Here we are also faced with another problem. Any input spike train, which fires the cell, will lead to complex "pre-post-pre-etc." combinations (Froemke & Dan, 2002), discussed also in Bi (2002). Our model can cope with these effects too, and we receive additional transitions from LTP to LTD or vice versa depending on the pre-post sequence, as shown in Figure 7C.

**4.2 Discussion of the Findings.** We believe that three of our findings could be of longer-lasting relevance for the understanding of synaptic learning, provided they withstand physiological scrutinizing: (1) the shape of the weight change curves heavily relies on the shape of the input functions (see Figures 5 and 8). (2) Differential Hebbian learning (STDP) can become similar to standard Hebbian learning (LTP) if the postsynaptic depolarization (i.e., the BP spike) rises shallow (see Figures 5A and 5B versus Figures 5F and 5G), (3) and weight growth can strongly change its characteristic in the course of learning if the membrane potential is locally dominated by the potential change arising from the plastic synapse itself (see Figure 7).

*4.2.1 Finding 1.* Physiological studies suggest that weight change curves can indeed have a widely varying shape (reviewed in Abbott & Nelson, 2000, and Roberts & Bell, 2002). In our study, both the NMDA characteristic and the characteristic of the depolarization source influence the shape of the weight change curve. The NMDA characteristic changes during

development, and in the ferret “young” NMDA channels are even slower than those found in adult animals (Roberts & Ramoa, 1999). We find that for “young” synapses, LTD strongly dominates (see Figure 6). Functionally this would make sense in helping to stabilize (Song, Miller, & Abbott, 2000; Rubin, Lee, & Sompolinsky, 2001; Kempster, Gerstner, & van Hemmen, 2001) an immature network, where false “inverse-causal” correlations could still be frequent.

Also, the shape of the membrane potential locally at the synapse is a source for differences in the shapes of the weight change curves. The physiological properties and morphology of dendritic trees will lead to a locally different active back-propagation or passive attenuation of the BP spike (Magee & Johnston, 1997; Larkum et al., 2001). It has been recently shown that synaptic plasticity in distal dendrites may be triggered by local  $\text{Na}^+$ - and/or  $\text{Ca}^{2+}$ - mediated dendritic spikes (Golding et al., 2002), which are usually slower than the BP spikes (Stuart, Spruston, Sakmann, & Häusser, 1997; Schiller, Schiller, Stuart, & Sakmann, 1997; Häusser, Spruston, & Stuart, 2000; Larkum et al., 2001). As a consequence of these different shapes of the depolarizing potentials, the resulting weight change curves would differ as well.

Many theoretical studies on STDP assume some kind of “generic” weight change curve that is applied regardless of the morphology of the neuron (Gerstner, Kempster, van Hemmen, & Wagner, 1996; Song et al., 2000; Kempster, Leibold, Wagner, & van Hemmen, 2001; Rubin et al., 2001). Others assume a gradually changing shape following, for example, the length of a dendrite without making specific assumptions about the parameters that lead to the different weight change curves (Panchev, Wermter, & Chen, 2002; Sterratt & van Ooyen, 2002). In our study, we argue that the shape of the inputs determines the shape of the weight change curves. It is interesting to consider that this way, local dendritic and spine properties would lead to different learning characteristics. For structures that are strongly electrically decoupled, the temporal structure and possible synchronization of the different inputs would be more important than the causality of pre- and postsynaptic signals. Note, however that the electrical (de-)coupling of spines is still a matter of debate (Koch, 1999; Kovalchuk, Eilers, Lisman, & Konnerth, 2000; Sabatini, Maravall, & Svoboda, 2001).

*4.2.2 Finding 2.* Several theoretical articles have shown that differential Hebb rules will lead to STDP-like behavior while plain (undifferentiated) Hebb rules will lead to temporally undirected LTP (Roberts, 1999; Xie & Seung, 2000; Roberts & Bell, 2002). Here we find that our differential Hebb rule can lead to plain LTP within rather wide correlation windows  $T$  as soon as the rising flank of our BP spike is shallow. In this case, the product of  $\hat{g}$  and  $V'$  remains positive for rather large negative temporal shifts of the postsynaptic signal. This finding indicates that at this model level, it is not necessary to assume fundamentally different mechanisms for LTP or STDP.

Yet from physiology, it is known that there are different intracellular processes involved for generating LTD or LTP. Furthermore, LTD is supposed to arise from low calcium influx, while LTP arises as soon as the calcium current is high (Nishiyama, Hong, Mikoshiba, Poo, & Kato, 2000). In an extended version, our model could be made compatible with these two aspects because the duration of the depolarization (hence  $V'$ ) and its temporal location with respect to the NMDA signal will determine how much calcium can flow, and this is different for the different values of  $T$ . One could implement two processes that are differently susceptible to these different calcium levels and thereby extend the model accordingly. The implications of being able to change an STDP to an LTP characteristic (or back) depending on the shape of the membrane potential are interesting from a theoretical point of view. Hebbian learning is usually associated with the extraction and condensation of relevant signals (Infomax principle, principal component analysis, Oja, 1982; Linsker, 1988), while STDP addresses the causality of synaptic events. It seems that the same substrate would support both principles and, in a similar way as discussed above, it could be the location at the dendrite that determines what kind of behavior is found. Possibly distal dendrites, where the potential changes can be shallow (Magee & Johnston, 1997; Larkum et al., 2001), discounting possible active processes, would experience LTP, proximal dendrites STDP. Also this can be a matter of further theoretical and experimental investigations.

*4.2.3 Finding 3.* We had found that weight growth can be linear or can contain a nonlinear transition when the positive feedback of the NMDA characteristic is dominant. This could again only happen at electrically more strongly decoupled parts of the membrane such as spines. There, small currents elicited by an active synapse will lead to large potential changes, which are required for this positive feedback effect. Such local potential changes cannot be measured anymore behind the spine neck because of its high resistance (Sabatini et al., 2001). In this case, the potential (change) that is the driving force of the calcium current would be strongly influenced by the local structure of the synaptic density, and correlation-based learning will take place between local inputs independent of the cell's soma (i.e., regardless of the firing of the cell).

**4.3 Comparison to Other Models.** A wide variety of models for STDP have been designed that can roughly be subdivided into two groups with different biophysical complexity. Some of them are spike based and others rate based.

Group 1 could be called abstract models. They assume a certain shape for a weight change curve as the learning rule (Gerstner et al., 1996; Song et al., 2000; Rubin et al., 2001; Kempster, Leibold et al., 2001; Gerstner & Kistler, 2002) that remains unchanged across the local properties of the cell. Thus, these studies cannot discuss cellular properties but focus on network effects

instead. One interesting finding obtained with these models was that STDP leads to self-stabilization of weights and rates in the network as soon as the LTD side dominates over the LTP side in the weight change curve (Song et al., 2000; Kempter, Gerstner, et al., 2001). In addition, it was found that such networks can store patterns (Abbott & Blum, 1996; Seung, 1998; Abbott & Song, 1999; Rao & Sejnowski, 2000; Fusi, 2002). More recently, these models have also been successfully applied to generate (i.e., to develop) some physiological properties such as map structures (Song & Abbott, 2001; Kempter, Leibold et al., 2001; Leibold & van Hemmen, 2002), direction selectivity (Buchs & Senn, 2002; Senn & Buchs, 2003) or temporal receptive fields (Leibold & van Hemmen, 2001). The biophysical realism of the used learning rules (really: weight change curves), however, must remain limited and cannot capture the wide variety of curves experimentally measured.

Group 2 could be called state variable models, to which we count our approach. Such models can adopt a rather descriptive approach (Abarbanel, Huerta, & Rabinovich, 2002), where appropriate functions are being fit to the measured weight change curves. Others are closer to the kinetic models in trying to fit phenomenological kinetic equations (Senn et al., 2000; Castellani et al., 2001; Karmarkar & Buonomano, 2002; Karmarkar, Najarian, & Buonomano, 2002; Shouval et al., 2002). Our approach tries to associate the used functions more closely to biophysics than that of Abarbanel et al. (2002), but, unlike some of the other models, we have not tried to fit any kinetic equations because model complexity substantially increases when doing so. As a consequence, our model is most closely related to the study of Rao and Sejnowski (2001). These authors used a variant of the TD learning rule to implement STDP. Dayan (2002) clarifies this issue and discusses that the rule of Rao and Sejnowski (2001) is rather a temporal difference rule between output activity values and not between prediction values as in the traditional TD rule. As a consequence, their rule is strongly related to our approach, and they also observe that the shape of the BP spike will influence the weight change curve. We have, however, replaced the 10 ms discretization used by Rao and Sejnowski (2001) for calculating the temporal difference by a real derivative (using 0.1 ms steps), and in our model the presynaptic activity is modeled as a conductance. This recently allowed us to solve the integral equation for the weight change (see equation 2.10) analytically for a slightly simplified set of conductance functions (Porr, Saudargiene, & Wörgötter, 2004).

Some of the other models implement a rather high degree of biophysical detail, including calcium, transmitter and enzyme kinetics (Senn et al., 2000; Castellani et al., 2001). The power of such models lies in the chance to understand and predict intra- or subcellular mechanism—for example, the aspect of AMPA receptor phosphorylation (Castellani et al., 2001), which is known to centrally influence synaptic strength (Malenka & Nicoll, 1999; Lüscher & Frerking, 2001; Song & Haganir, 2002).

The approaches of Shouval et al. (2002) as well as of Karmarkar and

co-workers (Karmarkar & Buonomano, 2002; Karmarkar et al., 2002) are a bit less detailed. Both models investigate the effects of different calcium concentration levels by assuming certain (e.g., exponential) functional characteristics to govern its changes. This allows them to address the question of how different calcium levels will lead to LTD or LTP (Nishiyama et al., 2000), and one of the models (Karmarkar & Buonomano, 2002) proposes to employ two different coincidence detector mechanisms to this end. An interesting aspect of our study and that of Rao and Sejnowski (2001) is that these models require only a single coincidence detector, because essentially the gradient of  $\text{Ca}^{2+}$  drives the learning when using a differential Hebbian learning rule and not the absolute  $\text{Ca}^{2+}$ -concentration (see Bi, 2002, for a detailed discussion of the gradient versus concentration model).

Both model types (Shouval et al., 2002; Karmarkar & Buonomano, 2002; Karmarkar et al., 2002) were designed to produce a zero crossing (transition between LTD and LTP) at  $T = 0$ , which is not always the case in the measured weight change curves, which show transitions between more LTP- and more LTD-dominated shapes depending on the cell type and the stimulation protocol (Roberts & Bell, 2002). The differential Hebb rule we employed leads to the observed results as the consequence of the fact that the derivative of any generic (unimodal) postsynaptic membrane signal (like a BP spike) will lead to a bimodal curve. The relative temporal location of the presynaptic depolarization signal with respect to the positive (or negative) hump of this bimodal curve will then determine if the convolution product is positive (weight growth) or negative (weight shrinkage). The model of Shouval et al. (2002) implicitly also assumes such a differential Hebbian characteristic by the bimodal shape of their  $\Omega$ -function, which they used to capture the calcium influence. This group also discussed, among other aspects, the role of the shape of the BP spike, and they concluded that a slow afterdepolarization potential (more commonly known as repolarization) must exist in order to generate STDP. This assumption is essentially similar to that of a slow fall time of the BP spike in our study. Thus, also in their study, the shape of the BP spike will influence the shape of the weight change curve. In general, they find that the LTP part of the curve is stronger than the LTD part. This observation would prevent self-stabilization of the activity in network models (Song et al., 2000; Kempter, Gerstner et al., 2001a), which require a larger LTD part for achieving this effect. Interestingly, however Shouval et al. (2002) find a second LTD part for larger positive values of  $T$ , which could perhaps be used to counteract such an activity amplification. In the hippocampus there is conflicting evidence if such a second LTD part exists for large  $T$  (Pike, Meredith, Olding, & Paulsen, 1999; Nishiyama et al., 2000).

## Acknowledgments

---

We acknowledge the support from SHEFC INCITE and EPSRC, GR/R74574/01. We are grateful to B. Graham, L. Smith, and D. Sterratt for their helpful comments on this manuscript.

## References

---

- Abarbanel, H. D. I., Huerta, R., & Rabinovich, M. I. (2002). Dynamical model of long-term synaptic plasticity. *Proc. Natl. Acad. Sci. (USA)*, *99*(15), 10132–10137.
- Abbott, L. F., & Blum, K. I. (1996). Functional significance of long-term potentiation for sequence learning and prediction. *Cereb. Cortex*, *6*, 406–416.
- Abbott, L. F., & Nelson, S. B. (2000). Synaptic plasticity, Taming the beast. *Nature Neurosci.*, *3*, 1178–1183.
- Abbott, L. S., & Song, S. (1999). Temporal asymmetric Hebbian learning, spike timing and neuronal response variability. In M. S. Kearns, S. Solla, & D. A. Cohn (Eds.), *Advances in neural information processing systems*, *11* (pp. 69–75). Cambridge, MA: MIT Press.
- Benett, M. R. (2000). The concept of long term potentiation of transmission at synapses. *Prog. Neurobiol.*, *60*, 109–137.
- Bi, G. Q. (2002). Spatiotemporal specificity of synaptic plasticity: Cellular rules and mechanisms. *Biol. Cybern.*, *87*, 319–332.
- Bi, G.-Q., & Poo, M. (2001). Synaptic modification by correlated activity, Hebb's postulate revisited. *Annu. Rev. Neurosci.*, *24*, 139–166.
- Bliss, T. V., & Gardner-Edwin, A. R. (1973). Long-lasting potentiation of synaptic transmission in the dentate area of the unanaesthetized rabbit following stimulation of the perforant path. *J. Physiol. (Lond.)*, *232*, 357–374.
- Bliss, T. V., & Lomo, T. (1970). Plasticity in a monosynaptic cortical pathway. *J. Physiol. (Lond.)*, *207*, 61P.
- Bliss, T. V., & Lomo, T. (1973). Long-lasting potentiation of synaptic transmission in the dentate area of the anaesthetized rabbit following stimulation of the perforant path. *J. Physiol. (Lond.)*, *232*, 331–356.
- Buchs, N. J., & Senn, W. (2002). Spike-based synaptic plasticity and the emergence of direction selective simple cells, Simulation results. *J. Comput. Neurosci.*, *13*, 167–186.
- Castellani, G. C., Quinlan, E. M., Cooper, L. N., & Shouval, H. Z. (2001). A biophysical model of bidirectional synaptic plasticity: Dependence on AMPA and NMDA receptors. *Proc. Natl. Acad. Sci. (USA)*, *98*(22), 12772–12777.
- Chechik, G., Meilijson, I., & Ruppin, E. (1998). Synaptic pruning in development: A computational account. *Neural Comp.*, *10*(7), 1759–1777.
- Dayan, P. (2002). Matters temporal. *Trends Cogn. Sci.*, *6*(3), 105–106.
- Debanne, D., Gähwiler, B. T., & Thompson, S. H. (1994). Asynchronous pre- and postsynaptic activity induces associative long-term depression in area CA1 of the rat hippocampus in vitro. *Proc. Natl. Acad. Sci. (USA)*, *91*, 1148–1152.
- Debanne, D., Gähwiler, B., & Thompson, S. (1998). Long-term synaptic plasticity between pairs of individual CA3 pyramidal cells in rat hippocampal slice cultures. *J. Physiol. (Lond.)*, *507*, 237–247.
- Feldman, D. (2000). Timing-based LTP and LTD at vertical inputs to layer II/III pyramidal cells in rat barrel cortex. *Neuron*, *27*, 45–56.
- Fortune, E. S., & Rose, G. J. (2001). Short-term synaptic plasticity as a temporal filter. *Trends Neurosci.*, *24*, 381–385.
- Froemke, R. C., & Dan, Y. (2002). Spike-timing-dependent synaptic modification induced by natural spike trains. *Nature*, *416*, 433–438.

- Fusi, S. (2002). Hebbian spike-driven synaptic plasticity for learning patterns of mean firing rates. *Biol. Cybern.*, *87*, 459–470.
- Gerstner, W., Kempter, R., van Hemmen, J. L., & Wagner, H. (1996). A neuronal learning rule for sub-millisecond temporal coding. *Nature*, *383*, 76–78.
- Gerstner, W., & Kistler, W. M. (2002). Mathematical formulations of Hebbian learning. *Biol. Cybern.*, *87*, 404–415.
- Giugliano, M., Bove, M., & Grattarola, M. (1999). Fast calculation of short-term depressing synaptic conductances. *Neural Comp.*, *11*, 1413–1426.
- Goldberg, J., Holthoff, K., & Yuste, R. (2002). A problem with Hebb and local spikes. *Trends Neurosci.*, *25*(9), 433–435.
- Golding, N. L., Staff, P. N., & Spruston, N. (2002). Dendritic spikes as a mechanism for cooperative long-term potentiation. *Nature*, *418*, 326–331.
- Gormezano, I., Kehoe, E. J., & Marshall, B. S. (1983). Twenty years of classical conditioning research with the rabbit. In J. M. Sprague & A. N. Epstein (Eds.), *Progress of psychobiology and physiological psychology* (pp. 198–274). Orlando, FL: Academic Press.
- Gustafsson, B., Wigstrom, H., Abraham, W. C., & Huang, Y.-Y. (1987). Long-term potentiation in the hippocampus using depolarizing current pulses as the conditioning stimulus to single volley synaptic potentials. *J. Neurosci.*, *7*, 774–780.
- Häusser, M., Spruston, N., & Stuart, G. J. (2000). Diversity and dynamics of dendritic signaling. *Science*, *11*, 739–744.
- Hebb, D. O. (1949). *The organization of behavior, A neuropsychological study*. New York: Wiley.
- Huemmeke, M., Eysel, U. T., & Mittmann, T. (2002). Metabotropic glutamate receptors mediate expression of LTP in slices of rat visual cortex. *Eur. J. Neurosci.*, *15*(10), 1641–1645.
- Karmarkar, U. R., & Buonomano, D. V. (2002). A model of spike-timing dependent plasticity, One or two coincidence detectors? *J. Neurophysiol.*, *88*, 507–513.
- Karmarkar, U. R., Najarian, M. T., & Buonomano, D. V. (2002). Mechanisms and significance of spike-timing dependent plasticity. *Biol. Cybern.*, *87*, 373–382.
- Kempter, R., Gerstner, W., & van Hemmen, J. L. (2001). Intrinsic stabilization of output rates by spike-based Hebbian learning. *Neural Comp.*, *13*, 2709–2741.
- Kempter, R., Leibold, C., Wagner, H., & van Hemmen, J. L. (2001). Formation of temporal-feature maps by axonal propagation of synaptic learning. *Proc. Natl. Acad. Sci. (USA)*, *98*(7), 4166–4171.
- Koch, C. (1999). *Biophysics of computation*. New York: Oxford University Press.
- Köhn, J., & Wörgötter, F. (1998). Employing the Z-transform to optimize the calculation of the synaptic conductance of NMDA and other synaptic channels in network simulations. *Neural Comp.*, *10*, 1639–1651.
- Kovalchuk, Y., Eilers, J., Lisman, J., & Konnerth, A. (2000). NMDA receptor-mediated subthreshold  $Ca^{2+}$ -signals in spines of hippocampal neurons. *J. Neurosci.*, *20*, 1791–1799.
- Krukowski, A. E., & Miller, K. D. (2001). Thalamocortical NMDA conductances and intracortical inhibition can explain cortical temporal tuning. *Nature Neurosci.*, *4*, 424–430.

- Larkum, M. E., Zhu, J. J., & Sakmann, B. (2001). Dendritic mechanisms underlying the coupling of the dendritic with the axonal action potential initiation zone of adult rat layer 5 pyramidal neurons. *J. Physiol. (Lond.)*, *533*, 447–466.
- Leibold, C., & van Hemmen, J. L. (2001). Temporal receptive fields, spikes, and Hebbian delay selection. *Neural Networks*, *14*(6-7), 805–813.
- Leibold, C., & van Hemmen, J. L. (2002). Mapping time. *Biol. Cybern.*, *87*, 428–439.
- Levy, W. B., & Steward, O. (1983). Temporal contiguity requirements for long-term associative potentiation/depression in the hippocampus. *Neurosci.*, *8*, 791–797.
- Linden, D. J. (1999). The return of the spike, Postsynaptic action potentials and the induction of LTP and LTD. *Neuron*, *22*, 661–666.
- Linsker, R. (1988). Self-organisation in a perceptual network. *Computer*, *21*(3), 105–117.
- Lüscher, C., & Frerking, M. (2001). Restless AMPA receptors, Implications for synaptic transmission and plasticity. *Trends Neurosci.*, *24*(11), 665–670.
- Mackintosh, N. J. (1974). *The psychology of animal learning*. Orlando, FL: Academic Press.
- Mackintosh, N. J. (1983). *Conditioning and associative learning*. Oxford: Oxford University Press.
- Magee, J. C., & Johnston, D. (1997). A synaptically controlled, associative signal for Hebbian plasticity in hippocampal neurons. *Science*, *275*, 209–213.
- Malenka, R. C., & Nicoll, R. A. (1999). Long-term potentiation—a decade of progress? *Science*, *285*, 1870–1874.
- Markram, H., Lübke, J., Frotscher, M., & Sakmann, B. (1997). Regulation of synaptic efficacy by coincidence of postsynaptic APs and EPSPs. *Science*, *275*, 213–215.
- Markram, H., & Tsodyks, M. (1996). Redistribution of synaptic efficacy between neocortical pyramidal neurons. *Nature*, *382*, 807–810.
- Martinez, J. L., & Derrick, B. E. (1996). Long-term potentiation and learning. *Annu. Rev. Psychol.*, *47*, 173–203.
- Nishiyama, M., Hong, K., Mikoshiba, K., Poo, M., & Kato, K. (2000). Calcium release from internal stores regulates polarity and input specificity of synaptic modification. *Nature*, *408*, 584–588.
- Oja, E. (1982). A simplified neuron model as a principal component analyzer. *J. Math. Biol.*, *15*(3), 267–273.
- Panchev, C., Wermter, S., & Chen, H. (2002). Spike-timing dependent competitive learning of integrate-and-fire neurons with active dendrites. In *Lecture Notes in Computer Science, Proc. Int. Conf. Artificial Neural Networks* (pp. 896–901). Berlin: Springer-Verlag.
- Pike, F. G., Meredith, R. M., Olding, A. A., & Paulsen, O. (1999). Postsynaptic bursting is essential for “Hebbian” induction of associative long-term potentiation at excitatory synapses in rat hippocampus. *J. Physiol. (Lond.)*, *518*, 571–576.
- Porr, B., Saudargiene, A., & Wörgötter, F. (2004). Analytical solution of spike-timing dependent plasticity based on synaptic biophysics. *Advances in neural information processing systems*, *16*. Cambridge, MA: MIT Press. In press.

- Porr, B., & Wörgötter, F. (2003a). Isotropic sequence order learning. *Neural Comp.*, *15*, 831–864.
- Porr, B., & Wörgötter, F. (2003b). Isotropic-sequence-order learning in a closed-loop behavioural system. *Proc. Roy. Soc. B*, *1811* (361), 2225–2244.
- Prokasy, W. F., Hall, J. F., & Fawcett, J. T. (1962). Adaptation, sensitization, forward and backward conditioning, and pseudo-conditioning of the GSR. *Psychol. Rep.*, *10*, 103–106.
- Rao, R. P. N., & Sejnowski, T. J. (2000). Predictive sequence learning in recurrent neocortical circuits. In S. Solla, T. K. Leen, & K.-R. Müller (Eds.), *Advances in neural information processing systems*, *12* (pp. 164–170). Cambridge, MA: MIT Press.
- Rao, R. P. N., & Sejnowski, T. J. (2001). Spike-timing-dependent Hebbian plasticity as temporal difference learning. *Neural Comp.*, *13*, 2221–2237.
- Roberts, E. B., & Ramoa, A. S. (1999). Enhanced NR2A subunit expression and decreased NMDA receptor decay time at the onset of ocular dominance plasticity in the ferret. *J. Neurophysiol.*, *81*, 2587–2591.
- Roberts, P. D. (1999). Computational consequences of temporally asymmetric learning rules. I. Differential Hebbian learning. *J. Comput. Neurosci.*, *7*(3), 235–246.
- Roberts, P. D., & Bell, C. C. (2002). Spike timing dependent synaptic plasticity in biological systems. *Biol. Cybern.*, *87*, 392–403.
- Rubin, J., Lee, D. D., & Sompolinsky, H. (2001). Equilibrium properties of temporally asymmetric Hebbian plasticity. *Phys. Rev. Lett.*, *86*(2), 364–367.
- Sabatini, B. L., Maravall, M., & Svoboda, K. (2001). Ca<sup>2+</sup> signaling in dendritic spines. *Current Opinion Neurobiol.*, *11*, 349–356.
- Schiller, J., Schiller, Y., & Clapham, D. E. (1998). Amplification of calcium influx into dendritic spines during associative pre- and postsynaptic activation: The role of direct calcium influx through the NMDA receptor. *Nat. Neurosci.*, *1*, 114–118.
- Schiller, J., Schiller, Y., Stuart, G., & Sakmann, B. (1997). Calcium action potentials restricted to distal apical dendrites of rat neocortical pyramidal neurons. *J. Physiol.*, *505*, 605–616.
- Senn, W., & Buchs, N. J. (2003). Spike-based synaptic plasticity and the emergence of direction selective simple cells: Mathematical analysis. *J. Comput. Neurosci.*, *14*, 119–138.
- Senn, W., Markram, H., & Tsodyks, M. (2000). An algorithm for modifying neurotransmitter release probability based on pre- and postsynaptic spike timing. *Neural Comp.*, *13*, 35–67.
- Seung, H. S. (1998). Learning continuous attractors in recurrent networks. In M. Kearns, M. Jordan, & S. Solla (Eds.), *Advances in neural information processing systems*, *10* (pp. 654–660). Cambridge, MA: MIT Press.
- Shouval, H. Z., Bear, M. F., & Cooper, L. N. (2002). A unified model of NMDA receptor-dependent bidirectional synaptic plasticity. *Proc. Natl. Acad. Sci. (USA)*, *99*(16), 10831–10836.
- Singer, W., & Gray, C. (1995). Visual feature integration and the temporal correlation hypothesis. *Annu. Rev. Neurosci.*, *18*, 555–586.

- Song, I., & Huganir, R. L. (2002). Regulation of AMPA receptors during synaptic plasticity. *Trends Neurosci.*, *25*(11), 578–588.
- Song, S., & Abbott, L. F. (2001). Cortical development and remapping through spike timing-dependent plasticity. *Neuron*, *32*, 1–20.
- Song, S., Miller, K. D., & Abbott, L. F. (2000). Competitive Hebbian learning through spike-timing-dependent synaptic plasticity. *Nature Neurosci.*, *3*, 919–926.
- Sourdet, V., & Debanne, D. (1999). The role of dendritic filtering in associative long-term synaptic plasticity. *Learning and Memory*, *6*, 422–447.
- Sterratt, D. C., & van Ooyen, A. (2002). Does morphology influence temporal plasticity. In J. R. Dorronsoro (Ed.), *ICANN 2002* (Vol. LNCS 2415, pp. 186–191). Berlin: Springer-Verlag.
- Stuart, G., Spruston, N., Sakmann, B., & Häusser, M. (1997). Action potential initiation and backpropagation in neurons of the mammalian central nervous system. *Trends Neurosci.*, *20*, 125–131.
- Sutton, R. S. (1988). Learning to predict by the methods of temporal differences. *Mach. Learn.*, *3*, 9–44.
- Sutton, R., & Barto, A. (1981). Towards a modern theory of adaptive networks, Expectation and prediction. *Psychol. Review*, *88*, 135–170.
- Teyler, T. J., & DiScenna, P. (1987). Long-term potentiation. *Annu. Rev. Neurosci.*, *10*, 131–161.
- Xie, X., & Seung, S. (2000). Spike-based learning rules and stabilization of persistent neural activity. In S. A. Solla, T. K. Leen, & K. R. Müller (Eds.), *Advances in neural information processing systems*, *12* (pp. 199–208). Cambridge, MA: MIT Press.
- Yuste, R., Majewska, A., Cash, S. S., & Denk, W. (1999). Mechanisms of calcium influx into hippocampal spines: Heterogeneity among spines, coincidence detection by NMDA receptors, and optical quantal analysis. *J. Neurosci.*, *19*, 1976–1987.